Uncertainty-Aware H_2 Control of a Wave Energy Converter Prototype

Josefredo Gadelha da Silva
Centre for Ocean Energy Research
Department of Electronic Engineering
Maynooth University,
Maynooth, W23 V5XH, Ireland
josefredo.silva.2024@mumail.ie

Marcio Junior Lacerda
School of Computing and Digital Media
London Metropolitan University
London, N7 8DB, UK
m.lacerda@londonmet.ac.uk

Erivelton Nepomuceno
Hamilton Institute
Centre for Ocean Energy Research
Department of Electronic Engineering
Maynooth University, W23 V5XH, Ireland
erivelton.nepomuceno@mu.ie

***Abstract*—This paper presents a data-driven robust control framework for wave energy converters. Unlike traditional model-based approaches that neglect uncertainties, the proposed method uses a data-driven model with polytopic uncertainty identified from experimental data of a Wavestar-type prototype. The control problem is cast as a convex semidefinite program with linear matrix inequalities (LMIs), enabling the synthesis of a robust H_2 controller that maximises average energy capture. Numerical results demonstrate that the proposed controller either outperforms or matches passive, reactive, and H_∞ strategies in energy absorption and control efficiency.**

I. Introduction

Maximising energy capture in wave energy converters (WECs) relies critically on effective control strategies, with controlled devices capable of absorbing up to four times more power than uncontrolled ones [1]. Most WEC controllers are based on linear potential flow theory (LPFT) [2], which assumes small motions and neglects nonlinear hydrodynamic effects, often leading to modelling inconsistencies such as negative power output [3].

These limitations reflect model uncertainty, a central challenge in WEC control alongside non-causality, physical constraints, and real-time implementability [4]. Although nonlinear hydrodynamic models offer improved accuracy, their computational cost restricts their use in control synthesis and real-time applications. As a result, linear models remain the practical choice, albeit at the expense of reintroduced uncertainty through model reduction and parameterisation.

Model uncertainty also constrains controller design. Classical impedance-matching control [2], while theoretically optimal, is non-causal and often assumes narrowband excitation, limiting its applicability in real ocean conditions. Consequently, practical implementations rely on approximate strategies such as passive or reactive controllers [5]. Recent experimental and data-driven modelling approaches aim to better capture hydrodynamic uncertainty [6], yet discrepancies between numerical and identified models persist, as evidenced by frequency-domain techniques such as empirical transfer function estimates (ETFE) [7].

Against this backdrop, this work proposes a novel causal, robust, uncertainty-aware control framework for WECs based on an H_2 performance criterion. A data-driven model with polytopic uncertainty enables a convex formulation via linear matrix inequalities (LMIs). By capturing the average energy response, the H_2 norm provides a physically meaningful objective for maximising energy extraction from stochastic ocean waves and, to the best of the authors' knowledge, represents the first application of an H_2-based robust control framework to WEC control.

II. Model Specification

This section presents the identification and parametrisation of a data-driven, uncertainty-aware, control-oriented model for a Wavestar-type WEC. The physical system is illustrated in Fig. 1 and the overall modelling workflow are illustrated in Fig. 2.

The experimental data are taken from the open-access SWELL dataset [8], obtained from a 1:20-scale Wavestar-type prototype at

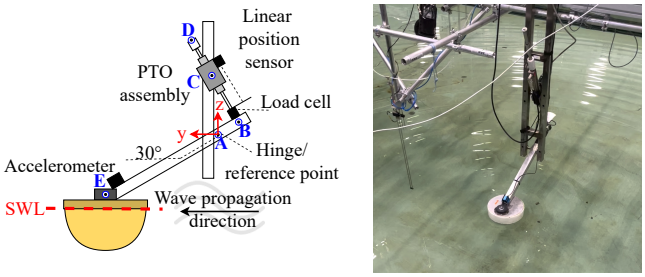

Fig. 1: Schematic and real prototype of the 1:20-scale Wavestar-type WEC (Aalborg University, May 2023).

Aalborg University (Fig. 1). A frequency-domain black-box identification approach is used to relate the wave-excitation torque about point A to the angular velocity response, where $\tau_A(t)$ is reconstructed from load-cell measurements and power take-off (PTO) kinematics (SWELL-Test 2) and $z(t) = \dot{\theta}_A(t)$ is obtained from Kalman-filter-based signal fusion (SWELL-Test 3).

To ensure broadband excitation of the dominant device dynamics, three white-noise sea states from the SWELL dataset (WNSS_1–WNSS_3) are considered. These inputs exhibit an approximately flat spectral density over the frequency range $[0.5,10]$ rad/s. Let $i \in \{1,2,3\}$ index the sea-state realisations. The corresponding frequency responses are estimated using empirical transfer function estimation (ETFE), $\widehat{G}_i(j\omega_k) = \frac{Z_i(\omega_k)}{F_{e,i}(\omega_k)}$, where $F_{e,i}(\omega_k)$ and $Z_i(\omega_k)$ denote the discrete Fourier transforms of the excitation torque and angular velocity, respectively. Spectral leakage and noise are mitigated by windowing and averaging over overlapping segments [9, 10, 11, 12].

A nominal frequency response is obtained as the complex average

$$\widehat{G}_0(j\omega_k) = \frac{1}{3}\sum_{i=1}^{3} \widehat{G}_i(j\omega_k), \tag{1}$$

which is subsequently approximated by a nominal state-space model $G_0(s)$. The fit is computed by minimising the squared error between the measured and modelled frequency responses,

$$\min_{G\in\mathcal{R}} \sum_k \left|\widehat{G}(j\omega_k) - \widehat{G}_0(j\omega_k)\right|^2, \tag{2}$$

where $\mathcal{R}$ denotes the class of continuous-time, stable, strictly proper LTI models, following standard practice in wave energy system identification [6, 13, 14, 15]. A fourth-order continuous-time realisation is them selected. Additionally, variability across the three sea states is captured through the magnitude envelope

$$\overline{G}(\omega_k) = \max_i \left|\widehat{G}_i(j\omega_k)\right|, \qquad \underline{G}(\omega_k) = \min_i \left|\widehat{G}_i(j\omega_k)\right|. \tag{3}$$

The frequency response functions were estimated using the H_1 estimator (`tfestimate`) with a periodic Hann window. For each experimental run, the segment length was set to L =

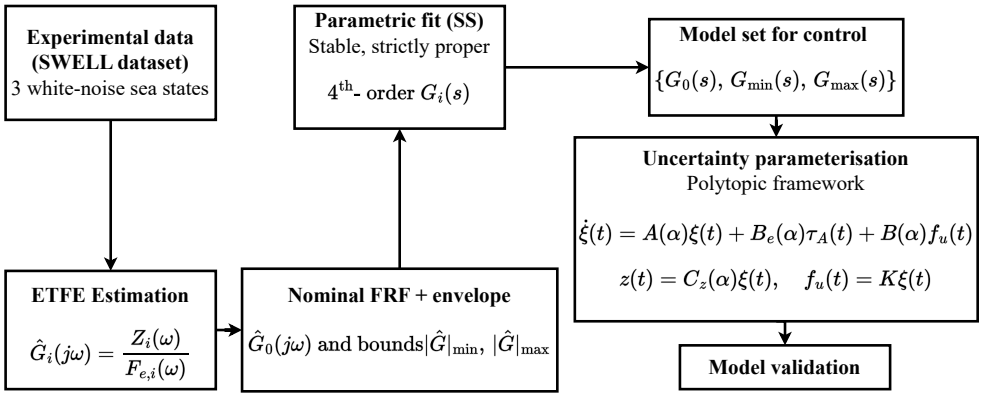

Fig. 2: System identification workflow and polytopic uncertainty parametrisation.

$\max\big(256, \operatorname{round}\big(\frac{N}{8}\big)\big)$, where N denotes the available data length after input–output alignment. Consecutive segments were overlapped by 50%, i.e., $N_{\text{overlap}} = \operatorname{round}(0.5\,L)$, and the FFT length was chosen as $N_{\text{FFT}} = 2^{\lceil \log_2 L \rceil}$. Accordingly, the number of Welch segments used in the averaging procedure is given by $K = 1 + \left\lfloor \frac{N-L}{L-N_{\text{overlap}}} \right\rfloor$, which is typically $K \approx 15$ for the settings adopted in this study. These parameters were applied consistently across all runs prior to coherence-based filtering and band selection.

Figure 3 presents the min–max envelope together with the nominal FRF and its continuous-time state-space fit, obtained using the identification procedure described in this section.

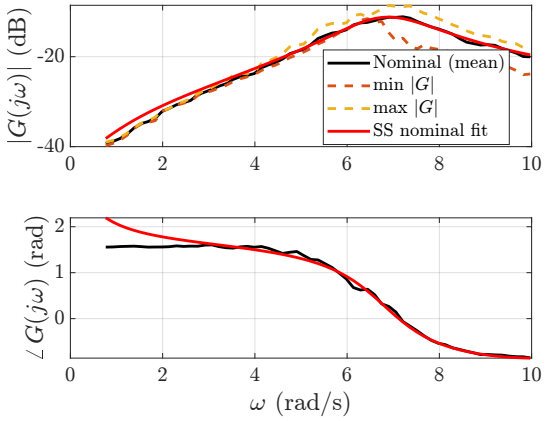

Fig. 3: Torque-to-angular-velocity frequency response from white-noise sea states: magnitude (top) and phase (bottom). The black line denotes the nominal FRF (mean), dashed lines the min-max envelope, and the red line the continuous-time state-space fit.

In this work, the state-space model is formulated as a controlled LTI system with polytopic uncertainty to parametrise the variability:

$$\begin{aligned} \dot{\xi}(t) &= A(\alpha)\xi(t) + B_e(\alpha)\tau_A(t) + B(\alpha)f_u(t), \\ z(t) &= C_z(\alpha)\xi(t) + D_{zu}(\alpha)f_u(t), \end{aligned} \tag{4}$$

where $\xi(t)$ is the system state, $\tau_A(t)$ the wave-excitation torque, $f_u(t) = K\xi(t)$ is the PTO control torque, K the robust control gain, and $z(t)$ the angular velocity. Each system matrix is written as a convex combination of vertex matrices, $\Xi(\alpha) = \sum_{i=1}^{N} \alpha_i \Xi_i, \quad \Xi \in \{A, B_e, B, C_z, D_{zu}\}$, with α belonging to the unit simplex $\Lambda_N = \alpha \in \mathbb{R}^N : \sum_{i=1}^{N} \alpha_i = 1,\ \alpha_i \geq 0$. In this work, the vertices correspond to the bounds of the frequency-response envelope in (3), yielding a two-vertex polytope ($\alpha \in \Lambda_2$).

The resulting closed-loop system is

$$\begin{cases} \dot{\xi}(t) = \big(A(\alpha) + B(\alpha)K\big)\xi(t) + B_e(\alpha)\tau_A(t), \\ z(t) = \big(C_z(\alpha) + D_{zu}(\alpha)K\big)\xi(t). \end{cases} \tag{5}$$

III. Robust Control Design

This section presents Lemma 1, which characterises the H_2 performance of continuous-time polytopic LTI systems. A finite set of LMIs, enforced at the polytope vertices, is used to compute a state-feedback gain that guarantees closed-loop stability for zero wave-excitation torque and provides an upper bound on the H_2 norm otherwise.

Definition 1. The H_2 norm from the impulsive input $\tau_A(t)$ to the output $z(t)$ of (4) is defined as

$$\|H_{ez}(s)\|_2 = \sqrt{\int_0^\infty \operatorname{Tr}\big(h(t)h(t)^\top\big)\, dt}, \tag{6}$$

where $h(t)$ denotes the impulse response, $\operatorname{Tr}(\cdot)$ the trace operator, and $A(\alpha)$ is Hurwitz with the system strictly proper [16].

Lemma 1. *Consider the system in* (4). *Given positive scalars β and δ, suppose there exist positive definite matrices $P(\alpha) \in \mathbb{R}^{n\times n}$ and $X \in \mathbb{R}^{n_z \times n_z}$, together with matrices $G \in \mathbb{R}^{n\times n}$, $Z \in \mathbb{R}^{n_u \times n}$, and $H(\alpha) \in \mathbb{R}^{n_u \times n_u}$, such that the LMIs* (7) *hold for all $\alpha \in \Lambda_N$. Then, the state-feedback gain $K = ZG^{-1}$ stabilises* (4) *and guarantees $\|H_{ez}\|_2 \leq \sqrt{\delta}, \quad \forall\, \alpha \in \Lambda_N$.*

$$\operatorname{Tr}(X) \leq \sqrt{\delta}, \tag{7a}$$

$$\begin{bmatrix} -X & C_z(\alpha)\,G + D_{zu}(\alpha)\,Z \\ \star & P(\alpha) - G - G^\top \end{bmatrix} \leq 0, \tag{7b}$$

$$\begin{bmatrix} A(\alpha)G + G^\top A(\alpha)^\top + B(\alpha)Z + Z^\top B(\alpha)^\top & & \\ \star & & \\ \star & & \end{bmatrix}$$
$$\begin{bmatrix} P(\alpha) - G^\top + \beta\big(A(\alpha)G + B(\alpha)Z\big) & B_e(\alpha)\,H(\alpha) \\ \beta\big(-G - G^\top\big) & 0 \\ 0 & \mathbf{I} - H(\alpha) - H(\alpha)^\top \end{bmatrix} \leq 0, \tag{7c}$$

Proof. Consider the closed-loop system (5). For zero initial conditions, the impulse response is $h(t) = C_{z,cl}(\alpha)e^{A_{cl}(\alpha)t}B_e(\alpha)$, which

yields

$$\|H_{ez}\|_2^2 = \mathrm{Tr}\big(C_{z,cl}(\alpha)W_c(\alpha)C_{z,cl}(\alpha)^\top\big), \tag{8}$$

where $W_c(\alpha)$ is the controllability Gramian satisfying $A_{cl}(\alpha)W_c(\alpha) + W_c(\alpha)A_{cl}(\alpha)^\top = -B_e(\alpha)B_e(\alpha)^\top$.

Let $P(\alpha) = P(\alpha)^\top \geq W_c(\alpha)$ satisfy the Lyapunov inequality

$$\begin{aligned} &A_{cl}(\alpha)P(\alpha) + P(\alpha)A_{cl}(\alpha)^\top + B_e(\alpha)B_e(\alpha)^\top \leq 0 \\ \Rightarrow &\begin{bmatrix}\mathbf{I} & A_{cl}(\alpha) & B_e(\alpha)\end{bmatrix} \begin{bmatrix} 0 & P(\alpha) & 0 \\ P(\alpha) & 0 & 0 \\ 0 & 0 & \mathbf{I}\end{bmatrix} \begin{bmatrix}\mathbf{I} \\ A_{cl}(\alpha)^\top \\ B_e(\alpha)^\top\end{bmatrix} \leq 0. \end{aligned} \tag{9}$$

Then,

$$\|H_{ez}\|_2^2 \leq \mathrm{Tr}\big(C_{z,cl}(\alpha)P(\alpha)C_{z,cl}(\alpha)^\top\big). \tag{10}$$

An equivalent condition to (10) is given by

$$\begin{aligned} &\|H_{ez}\|_2^2 \leq \mathrm{Tr}(X), \quad \text{s.t.} \\ &C_{z,cl}(\alpha)P(\alpha)C_{z,cl}(\alpha)^\top - X \leq 0, \\ \Rightarrow\ &\begin{bmatrix}\mathbf{I} & C_{z,cl}(\alpha)\end{bmatrix} \begin{bmatrix}-X & 0 \\ 0 & P(\alpha)\end{bmatrix} \begin{bmatrix}\mathbf{I} \\ C_{z,cl}(\alpha)^\top\end{bmatrix} \leq 0, \end{aligned} \tag{11}$$

where $X \in \mathbb{R}^{n_z \times n_z}$. Applying Finsler's lemma [17] to (9) and (11) yields, respectively,

$$\begin{aligned} &\begin{bmatrix} 0 & P(\alpha) & 0 \\ P(\alpha) & 0 & 0 \\ 0 & 0 & \mathbf{I}\end{bmatrix} + \begin{bmatrix}X_1 & X_4 \\ X_2 & X_5 \\ X_3 & X_6\end{bmatrix} \begin{bmatrix}A_{cl}(\alpha)^\top & B_e(\alpha)^\top \\ -\mathbf{I} & 0 \\ 0 & -\mathbf{I}\end{bmatrix}^\top \\ &\quad + \begin{bmatrix}A_{cl}(\alpha) & B_e(\alpha) \\ -\mathbf{I} & 0 \\ 0 & -\mathbf{I}\end{bmatrix} \begin{bmatrix}X_1^\top & X_4^\top \\ X_2^\top & X_5^\top \\ X_3^\top & X_6^\top\end{bmatrix}^\top \leq 0, \end{aligned} \tag{12}$$

and

$$\begin{aligned} &\begin{bmatrix}-X & 0 \\ 0 & P(\alpha)\end{bmatrix} + \begin{bmatrix}-V \\ -J\end{bmatrix} \begin{bmatrix}-C_{z,cl}(\alpha)^\top & \mathbf{I}\end{bmatrix} \\ &\quad + \begin{bmatrix}-C_{z,cl}(\alpha) \\ \mathbf{I}\end{bmatrix} \begin{bmatrix}-V^\top \\ -J^\top\end{bmatrix}^\top \leq 0 \Rightarrow \\ &\begin{bmatrix}-X + VC_{z,cl}(\alpha)^\top + C_{z,cl}(\alpha)V^\top & -V + C_{z,cl}(\alpha)J^\top \\ -V^\top + JC_{z,cl}(\alpha)^\top & P(\alpha) - J - J^\top\end{bmatrix} \leq 0. \end{aligned} \tag{13}$$

The LMIs (7b)–(7c) are recovered by applying the substitutions $V = 0$, $J = G^\top$, $X_1 = G^\top$, $X_2 = \beta G^\top$, $X_6 = H(\alpha)^\top$, $X_3 = X_4 = X_5 = 0$, and $Z = KG$. □

The power absorbed by the WEC is $P_{\mathrm{mec}}(t) = \tau_A(t)z(t)$, and the control objective is to maximise the extracted energy $E = \int_0^T P_{\mathrm{mec}}(t)\,dt = \int_0^T \tau_A(t)z(t)\,dt$, where T denotes the time horizon. In this work, the LMIs (7b)–(7c) impose an upper bound on the H_2 norm from $\tau_A(t)$ to $z(t)$. Energy maximisation is achieved by relaxing δ, thereby increasing the variance of the angular-velocity response to stochastic wave excitation within the operating frequency band.

IV. Numerical Results

This section presents a numerical assessment of the simulation results obtained by applying the robust H_2 controller described in the previous section to the system characterised in Section II. The controller gain was computed by formulating and solving the LMI conditions using the YALMIP parser ([18]), the ROLMIP toolbox ([19]), and the SeDuMi solver ([20]). In this work, the optimisation was limited to the parameters β and δ, which were explored using a logarithmic grid. The search intervals were set to $[10^{-5},10^{0}]$ for β and $[10^{0},10^{10}]$ for δ, based on practical experience indicating that feasible LMI solutions are most likely to be obtained within these ranges.

All the cases presented in this section refer to the nominal model, $G_0(s)$, introduced in Section II. For validation, three irregular sea states from the SWELL dataset, defined by JONSWAP spectra, are considered (Table I). These conditions differ from those used for identification and include both narrow- and broadband cases, allowing assessment of the controller's performance under realistic, stochastic wave excitation. Benchmark passive and reactive control results provided in SWELL are used for comparison.

To demonstrate the effectiveness of the proposed controller, Fig. 4 compares the excitation torque and the resulting angular position of the WEC in uncontrolled and H_2-controlled cases. For the same excitation, the controlled system exhibits greater motion amplitude, consistent with the goal of WEC control, to amplify motion and thereby increase energy absorption from the waves.

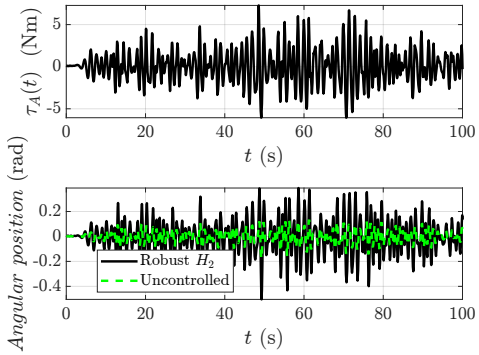

Fig. 4: Time snippet of the excitation torque (top), and time-domain response of the WEC under both uncontrolled and controlled conditions (bottom), the latter governed by the proposed robust H_2 controller for ISS1.

Additionally, the performance of the proposed H_2 controller is benchmarked against the passive and reactive controllers [5], as well as a classical robust approach, the H_∞ controller, whose design conditions are available in ([21]). Table II summarises the tuning parameters of all controllers.

Figure 5 compares the controller performance in terms of WEC output velocity and control force. It can be seen that, while requiring a smaller control effort, the H_2 controller achieves superior performance in maximising WEC motion compared with the other approaches.

As none of the existing non-optimisation-based WEC controllers can effectively handle hard constraints [22], a common approach in the case of reactive and passive controllers is to tune them by approximating the values derived from the IM principle (Table II), thereby avoiding physical constraint violations. Accordingly, Fig. 6 presents the results of Test 4 from the SWELL dataset, corresponding to the passive and reactive cases without such violations, along with the H_∞ and H_2 controllers. Table III summarises the total energy produced in this experiment. From the results, it can be concluded that the H_2 controller behaves similarly to the reactive controller, which typically injects power back into the system during parts of the cycle [23]. Across all sea states, the H_2 controller generated more energy than the H_∞, reactive, and passive cases. As expected, the H_2 controller outperformed the H_∞ controller, as it minimises the average energy of the system response to stochastic wave excitations,

TABLE I: Irregular sea-state conditions from the SWELL dataset used for controller validation.

Layout	Sea state	Test file	Height H_s [m]	Period T_p [s]	Peakedness γ	Length [s]
L0	ISS–1	`11_ISS1_1`	0.063	1.412	3.3	300
L0	ISS–2	`13_ISS2_1`	0.104	1.836	3.3	300
L0	ISS–3	`15_ISS3_1`	0.0208	0.988	1	300

Paths follow `Tests/L0/(11{15)_ISS(1{3)_1.mat`.

TABLE II: Controller tuning parameters.

Parameter	H_2 Controller	H_∞ Controller
β	1.0×10^{-1}	1.0×10^{-2}
δ	1.0×10^{8}	1.0×10^{10}
Polynomial degree $P(\alpha)$	3	0
Polynomial degree $H(\alpha)$	15	0

	Passive Controller	Reactive Controller	
ISSs	K_P	K_p	K_i
ISS1	3.6103	0.8983	−15.5601
ISS2	5.7974	0.7729	−19.6628
ISS3	1.3681	1.1310	−4.8946

Note: The polynomial degrees refer to the homogeneous dependence of the decision variables on the scheduling parameter α, as defined by the the ROLMIP toolbox ([19])

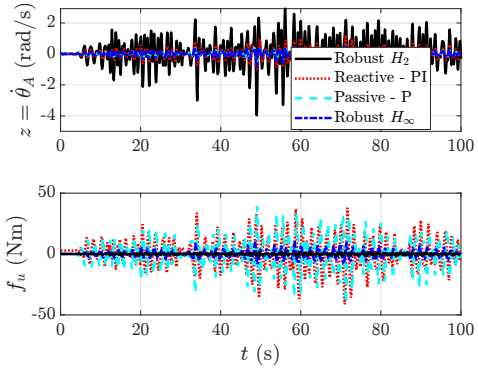

Fig. 5: Comparison of the proposed robust H_2 controller with the passive, reactive, and H_∞ strategies for ISS2. The top plot shows a time snippet of the WEC angular velocity, and the bottom plot the corresponding control torque. The H_2 controller yields greater motion amplitude with lower control effort.

whereas the H_∞ formulation is designed to guarantee performance only under worst-case conditions.

TABLE III: Energy generated [J].

Controller	ISS1	ISS2	ISS3
H_∞	30.7462	55.4733	6.7178
Passive	69.0878	145.0654	13.5941
Reactive	159.5929	217.1432	13.2706
H_2	257.6155	413.6734	56.3616

V. Conclusions

The results demonstrate the effectiveness of the proposed robust H_2 controller for wave energy conversion. Compared with passive, reactive, and robust H_∞ strategies, the H_2 controller achieved improved energy capture while maintaining balanced control effort and compliance with physical limits. The hypothesis that the H_2 formulation performs well in wave energy systems, by accounting for the average contribution of excitation frequencies, was confirmed. In contrast to H_∞ control, which targets worst-case scenarios, the H_2 approach provides an effective trade-off between energy absorption and robustness under stochastic sea states. These results were obtained by tuning only two parameters, β and δ, highlighting

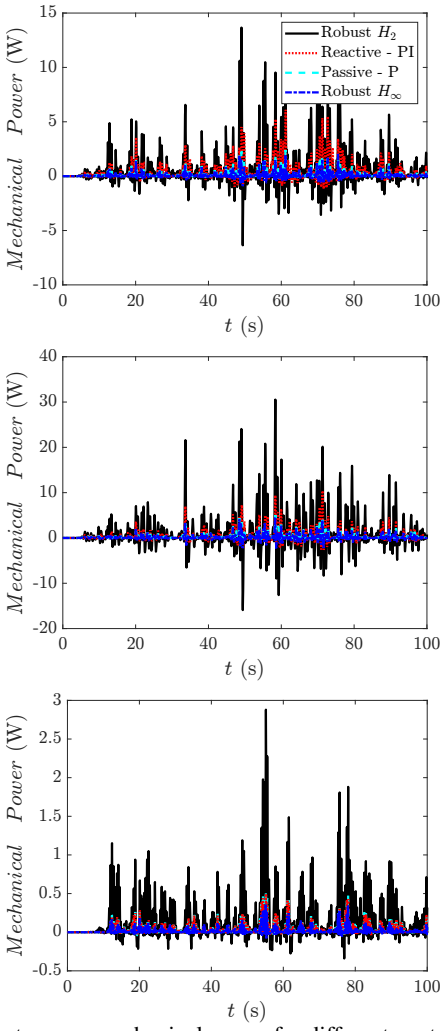

Fig. 6: Instantaneous mechanical power for different control strategies and sea states. The passive and reactive cases correspond to those available in the SWELL dataset ([8]), where no physical violations occur.

the method's simplicity and practical applicability. The study also underlines the potential of data-driven control in mitigating modelling uncertainties and limitations inherent to model-based frameworks. Future work will extend the framework to incorporate explicit state constraints and PTO dynamics, and benchmark the approach against other advanced WEC control strategies.

Acknowledgment

This work was supported by Taighde Éireann – Research Ireland (Grant 21/FFP-P/10065). For Open Access, the author has applied a CC BY public copyright licence to any Author Accepted Manuscript arising from this submission. E. Nepomuceno was also supported by CNPq, Brazil (Grant 444154/2024-8). Josefredo Gadelha da Silva gratefully acknowledges the financial support of the Graduate Research Academy at Maynooth University.

References

[1] J. V. Ringwood, S. Zhan, and N. Faedo, "Empowering wave energy with control technology: Possibilities and pitfalls," *Annual Reviews in Control*, vol. 55, pp. 18–44, 2023.

[2] J. Falnes, *Ocean Waves and Oscillating Systems: Linear Interactions Including Wave-Energy Extraction*. Cambridge University Press, 2002.

[3] C. Windt, N. Faedo, M. Penalba, F. Dias, and J. V. Ringwood, "Reactive control of wave energy devices – the modelling paradox," *Applied Ocean Research*, vol. 109, p. 102574, 2021.

[4] D. Ning and B. Ding, *Modelling and optimization of wave energy converters*. CRC Press, 2022.

[5] N. Faedo, F. Carapellese, E. Pasta, and G. Mattiazzo, "On the principle of impedance-matching for underactuated wave energy harvesting systems," *Applied Ocean Research*, vol. 118, p. 102958, 2022.

[6] N. Faedo and M. L. Celesti, "On the role of modelling uncertainty in optimal control and performance assessment of wave energy conversion systems," in *ISOPE International Ocean and Polar Engineering Conference*, pp. ISOPE–I, ISOPE, 2024.

[7] M. Farajvand, V. Grazioso, D. García-Violini, and J. V. Ringwood, "Uncertainty estimation in wave energy systems with applications in robust energy maximising control," *Renewable Energy*, vol. 203, pp. 194–204, 2023.

[8] N. Faedo, Y. Peña-Sanchez, E. Pasta, G. Papini, F. D. Mosquera, and F. Ferri, "Swell: An open-access experimental dataset for arrays of wave energy conversion systems," *Renewable Energy*, vol. 212, pp. 699–716, 2023.

[9] E. C. Levy, "Complex-curve fitting," *IRE Transactions on Automatic Control*, vol. 4, no. 1, pp. 37–43, 1959.

[10] P. D. Welch, "The use of fast fourier transform for the estimation of power spectra: A method based on time averaging over short, modified periodograms," *IEEE Transactions on Audio and Electroacoustics*, vol. 15, no. 2, pp. 70–73, 1967.

[11] B. Gustavsen and A. Semlyen, "Rational approximation of frequency domain responses by vector fitting," *IEEE Transactions on Power Delivery*, vol. 14, no. 3, pp. 1052–1061, 1999.

[12] T. McKelvey, H. Akçay, and L. Ljung, "Subspace-based identification from frequency response data," *IEEE Transactions on Automatic Control*, vol. 41, no. 7, pp. 960–979, 1996.

[13] L. Ljung, *System Identification: Theory for the User*. Upper Saddle River, NJ: Prentice Hall PTR, 2nd ed., 1999.

[14] R. Pintelon and J. Schoukens, *System Identification: A Frequency Domain Approach*. Hoboken, NJ: Wiley-IEEE Press, 2nd ed., 2012.

[15] M. L. Celesti, F. Ferri, and N. Faedo, "Experimental modelling uncertainty quantification for a prototype wave energy converter," in *2024 European Control Conference (ECC)*, pp. 1546–1551, 2024.

[16] L. H. Salame de Andrade and C. M. Agulhari, "Robust mixed h2/h∞ control of an nonlinear multivariable system," in *2016 12th IEEE International Conference on Industry Applications (INDUSCON)*, pp. 1–8, 2016.

[17] M. C. de Oliveira and R. E. Skelton, "Stability tests for constrained linear systems," in *Perspectives in Robust Control* (S. O. Reza Moheimani, ed.), vol. 268 of *Lecture Notes in Control and Information Science*, pp. 241–257, New York, NY: Springer-Verlag, 2001.

[18] J. Löfberg, "Yalmip : A toolbox for modeling and optimization in matlab," in *In Proceedings of the CACSD Conference*, (Taipei, Taiwan), 2004.

[19] C. M. Agulhari, A. Felipe, R. C. L. F. Oliveira, and P. L. D. Peres, "Algorithm 998: The Robust LMI Parser — A toolbox to construct LMI conditions for uncertain systems," *ACM Transactions on Mathematical Software*, vol. 45, p. 36:1–36:25, August 2019.

[20] J. F. Sturm, "Using sedumi 1.02, a MATLAB toolbox for optimization over symmetric cones," *Optimization Methods and Software*, vol. 11, no. 1-4, pp. 625–653, 1999.

[21] J. G. da Silva, M. J. Lacerda, A. L. J. Bertolin, T. Nazaré, M. Costa, and E. Nepomuceno, "H∞ control co-design for uncertain polytopic systems," *ASME Letters in Dynamic Systems and Control*, vol. 5, p. 030905, 05 2025.

[22] P. Fornaro, Z. Lin, *et al.*, "Symphony: The ultimate wave energy controller," in *Proceedings of the European Wave and Tidal Energy Conference*, vol. 16, 2025.

[23] F. Fusco and J. V. Ringwood, "A simple and effective real-time controller for wave energy converters," *IEEE Transactions on Sustainable Energy*, vol. 4, no. 1, pp. 21–30, 2013.